Ice adhesion of PDMS surfaces with balanced elastic and water-repellent properties

Pablo F. Ibáñez-Ibáñez, F. Javier Montes Ruiz-Cabello, Miguel A. Cabrerizo-Vílchez, Miguel A. Rodríguez-Valverde *

Laboratory of Surface and Interface Physics, Department of Applied Physics, University of Granada, Campus de Fuentenueva; Es-18071 Granada, Spain

HIGHLIGHTS

- PDMS-based coatings for deicing were prepared with wide-ranging properties.
- Shear stresses developed on elastomeric surfaces allow to decrease ice adhesion strength.
- Impact of the elasticity on ice adhesion is more noticeable under shear forces.
- Impact of the hydrophobicity on ice adhesion is more noticeable under tensile forces.
- Proper balance between surface and bulk properties leads to super low ice-adhesion.

GRAPHICAL ABSTRACT
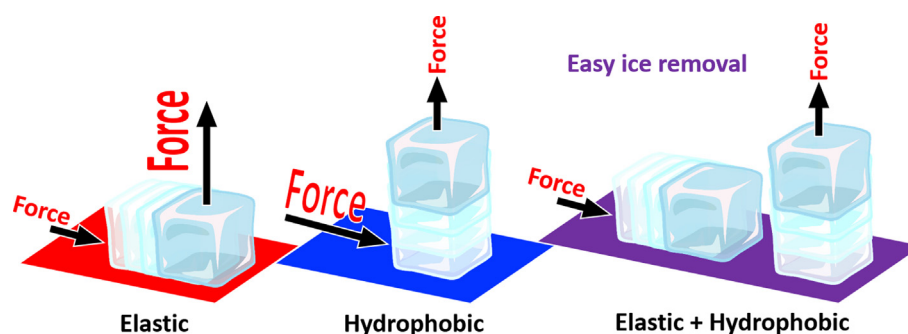
ABSTRACT

Hypothesis: Ice adhesion to rigid materials is reduced with low energy surfaces of high receding contact angles. However, their adhesion strength values are above the threshold value to be considered as icephobic materials. Surface deformability is a promising route to further reduce ice adhesion.
Experiments: In this work, we prepared elastomer surfaces with a wide range of elastic moduli and hydrophobicity degree and we measured their ice adhesion strength. Moreover, we also explored the deicing performance of oil-infused elastomeric surfaces. The ice adhesion was characterized by two detachment modes: tensile and shear.
Findings: The variety of elastomeric surfaces allowed us to simultaneously analyze the ice adhesion dependence with deformability and contact angle hysteresis. We found that the impact of these properties depends on the detachment mode, being deformability more important in shear mode and hydrophobicity more relevant in tensile mode. In addition, oil infusion further reduces ice adhesion due to the interfacial slippage. From an optimal balance between deformability and hydrophobicity, we were able to identify surfaces with super-low ice adhesion.

1. Introduction

Icephobic materials are being developed due to their applicability in different fields such as ski facilities, solar energy, wind energy, aeronautics or even offshore oil rigs [1–4]. Despite the recent advances in icephobic surfaces, a low-energy and

* Corresponding author.
E-mail address: marodri@ugr.es (M.A. Rodríguez-Valverde).

long-lasting solution is still missing. Currently, most of the anti/de-icing systems used in real world applications are active systems that require high energy consumption or the employment of unsustainable chemicals. Synergy between hydrophobic materials and active systems will allow to save greatly heating energy [5,6]. However, the research community is mostly focused on the development of passive surfaces that mitigate ice formation or reduce ice adhesion below 10 kPa, allowing the ice removal by natural forces [7]. Superhydrophobic surfaces have shown very good properties for repelling supercooled water drops and for the delay of surface freezing [8,9]. SLIPS (Slippery Liquid-Infused Porous Surfaces) also reveal anti-frost performance and effortless de-icing (low ice-adhesion) [10]. However, durability is an issue for this kind of surfaces [11]. On the other hand, deformable surfaces have shown low ice adhesion and good durability in icing-deicing cycles [12], unlike SLIPS. For these reasons, elastic materials are currently a promising solution to mitigate ice adhesion. In addition, these materials can be used to fabricate other type of release surfaces, such as oil-infused polymer matrix [13] or surfaces impregnated with anti-icing liquids (ethanol, salted water) [14].

In this work, we prepared a wide selection of PDMS surfaces and oil-infused PDMS surfaces using silicone oil. We measured the ice adhesion from two detachment modes and analyzed their relation with elasticity and hydrophobicity. We also analyzed the removal mechanisms of ice. Super-low ice adhesion was successfully found.

2. Materials and methods

2.1. Surface preparation

To study the ice adhesion to non-rigid surfaces, we prepared different PDMS surfaces. We used Sylgard 184 (DOWSIL), a two-component PDMS kit, to fabricate silicone-based surfaces with different elastic moduli and wetting properties by varying the w/w ratios between curing agent and polymer base (3:1, 2:1, 3:2, 1:1, 1:2, 1:5, 1:10, 1:15, 1:20, 1:25, 1:30, 1:40, 1:50). The mixtures were vigorously stirred by hand, and degassed in a vacuum chamber. Then, approx. 4.2 mL of the mixture were poured into a mold with a glass slide (76 × 25 mm², LineaLab) at the bottom to produce a 2 mm thickness surface. Then, the molds were let to cure for 48 h at room temperature (23 °C) and then introduced in an oven at 100 °C for 1 h. We also prepared two-layer PDMS surfaces to explore low elastic moduli and low wettability. For this purpose, using a spin coating (Laurell WS-650MZ-23NPP/LITE), PDMS 1:30, 1:40 and 1:50 surfaces were further coated with a thin film of PDMS 1:5, 1:2 and 1:1 mixtures respectively. Then, they were introduced in oven at 100 °C for 1 h to ensure the complete crosslinking. The thin films (58–77 μm) were made using 0.6 mL of PDMS and setting the spin coating at 1000 rpm for 1 min. In addition, a 1:25 PDMS surface was treated with UV light (Novascan PSD ProSeries) during 4 h to alter its wetting properties. All PDMS surfaces were rinsed with ethanol and Milli-Q water (Quantum EX, Millipak Express 20) prior to use.

Oil-infused elastomeric surfaces were also prepared. For this purpose, PDMS with different ratios (1:1, 1:2, 1:10, 1:30) were further mixed with different percentages in weight of silicone oil (Sigma-Aldrich 100 cSt): 5, 10, 20, 35, 50 %. Next, the samples were stirred, degassed, and cured using the same protocol detailed above. The oil-infused surfaces were rinsed with Milli-Q water prior to use.

We prepared three control surfaces: untreated aluminum (hydrophilic), aluminum with a hydrophobic coating, and superhydrophobic aluminum. Aluminum 6061 sheets supplied by Pyltin (Spain) were cleaned with acetone and ethanol, rinsed with

distilled water and dried with a jet of compressed air. To deposit a hydrophobic coating, aluminum sheets were introduced into an air plasma cleaner (EMITECH K1050X) for 10 min at 100 W for further cleaning and surface activation. Then a thin layer of fluoropolymer (DuPont AF 1600 dissolved in FC-72 (3 M) solvent at ratio 1/20 (v/v)) was sprayed over it. A second layer was sprayed after 30 min drying at room temperature and then introduced in oven at 100 °C for 10 min. To fabricate superhydrophobic surfaces, aluminum sheets were previously etched in 4 M HCL (HCL 37%, Scharlau), then rinsed with water, dried, cleaned in air plasma and finally coated with the fluoropolymer film as previously described for un-etched aluminum [15,16].

2.2. Surface characterization

2.2.1. Surface roughness

The surface roughness was characterized with a White Light Confocal Microscope (PLμ 2300, Sensofar). The magnification was 50×, the scan area was 285.38 × 209.62 μm², and the measured parameters were the average roughness (R_a) and the root mean square roughness (R_q or rms), averaged over four measurements.

2.2.2. Elastic moduli

To characterize the elastic moduli (E) of the PDMS surfaces we used a cylindrical probe attached to a dynamometer (IMADA ZTA-200 N, ZTA-20 N), which moves with a motorized linear stage (IMADA MH2-500 N-FA). The probe (13.00 ± 0.05 mm diameter) compresses the 2-mm thick PDMS surface at 10 mm/min, and the force–displacement curve is recorded by the software (Force Recorder). This way, the elastic moduli were calculated as $E = (F/A)/(\Delta L/L) = (F/\Delta L)(L/A)$ [17], where L is the surface thickness, A the probe area and $(F/\Delta L)$ is the slope of the linear part of the force–displacement curve. At least four measurements were performed for each surface. A drop of cutting fluid was applied between the PDMS surface and the probe to avoid any barreling effect and to reduce inaccuracies [18]. Barreling happens when the compressed material expands more easily at the center than at the edge due to the friction forces developed between the compressed material and the probe. The name barreling comes from the shape that compressed cylindrical materials adopt. No cutting oil was applied on oil-infused PDMS surfaces to avoid contamination.

2.2.3. Wetting properties

The wetting properties were characterized by means of the water contact angle (CA). We employed two different techniques, the tilting plate (lab-designed [19]) for the oil-infused PDMS surfaces and the growing-shrinking sessile drop (lab-designed [20]) for the PDMS surfaces. In the tilting plate, a sessile drop (50 μL) is deposited over the surface and the advancing and receding contact angles (ACA and RCA) are measured as the downhill and uphill contact angles of the drop at incipient motion, once the surface is tilted at the sliding angle (SA). More details about this method can be found in literature [19,21,22]. The inclination speed is 5°/s and the frame rate 16 fps. The growing-shrinking drop method allows to change the volume of a sessile drop throughout a hole drilled to the surface. The ACA is measured while the contact line advances (growing) and the RCA is measured when the contact line recedes (shrinking). The initial drop volume is 10 μL and the injected/extracted volume is 150 μL with a quadratic flow rate [20]. At least three measurements were performed for each surface. The PDMS surfaces with very low RCA, and consequently high SA, cannot be characterized with the tilting plate. To drill a hole to the oil-infused surfaces typically requires the use of cutting fluid. That may lead to undesired contamination, so the growing-shrinking drop method is not recommended.

2.3. Ice adhesion (pull-off) test

We characterized the ice adhesion in two modes: the tensile and shear adhesion (see supplementary Figure S1). The force is applied by the motorized linear stage at 10 mm/min (0.167 mm/s). The two modes of ice detachment are qualitatively different and provide complementary information. To produce the ice, we first placed a hollow Teflon cylinder on the surface at room temperature. Then, the cylinder was filled with 1 mL of Milli-Q water. The internal diameter was 9.86 ± 0.12 mm (area 76.4 ± 1.9 mm^2) and the water level was about 13 mm. Then, the surface was placed inside the freezing chamber and let to freeze at -10 °C for 90 min (RH 40–50 % during freezing), up to the complete water solidification. Once frozen, the surfaces were fixed to a platform placed inside the freezing chamber. In the tensile mode, with the surface placed horizontally, a hook joined by a thread to the dynamometer was attached to the top of the cylinder. This way, the cylinder (ice) is detached from the surface while the hook is pulled up. In the shear mode, with the surface placed vertically, a ring was placed around the cylinder near to the surface, at a distance of 1.0 ± 0.5 mm. Now, the detachment force is parallel to the surface. The software provides the force–time plot and from it, we record the peak force. With the peak force we calculate the ice adhesion strength (force per area unit, *IceAdhesioStrength = Force/Area*) like a normal or shear stress, accordingly. The final values were averaged over at least four measurements. All the ice adhesion tests were conducted inside the freezer.

3. Results

3.1. Rigid surfaces

The results for the control (metal-based) surfaces are summarized in Table 1. As expected, the (smooth) hydrophobic surface presents lower ice adhesion strength than the (smooth) hydrophilic surface. The superhydrophobic surfaces with significant water repelling properties (more than 15 bounces in bouncing drop experiments [15]) develop higher ice adhesion than the hydrophilic surface, due to the mechanical interlocking enhanced by the roughness. The morphology of these control surface can be observed in SEM images of our previous work [15].

3.2. Elastic PDMS surfaces

The PDMS surfaces show a roughness degree, monitored by the R_a values, mostly within the range 20–100 nm (see supplementary Table S1). They can be considered as smooth surfaces, because their roughness magnitude is lower than the one observed for the control aluminum surface, or at least comparable to it. Since surface roughness of all PDMS surfaces is very small, we ignored the effect of roughness in both wetting and ice adhesion properties.

The elastic response of the PDMS surfaces is characterized by means of the elastic moduli (E) showed in Fig. 1. There is a maximum value of elastic modulus for both the 1:10 (the ratio recommended by the supplier) and 1:5 surfaces. Far from the peak observed at 1:10, the elastic modulus decreases substantially. It is well-known that the resistance of PDMS is maximum for 1:10 ratio, for example there is the maximum strain strength [23].
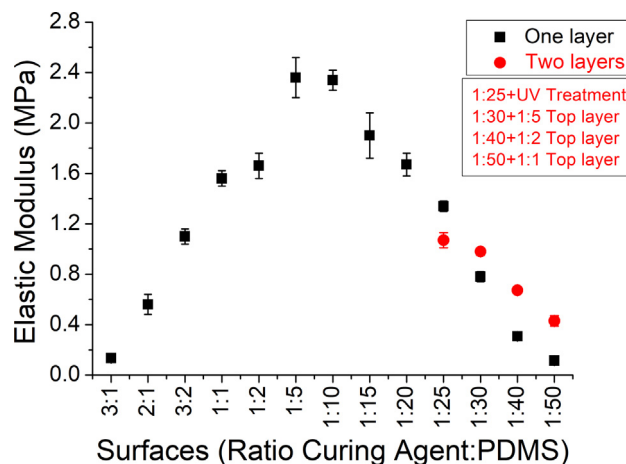

Fig. 1. Elastic moduli of the PDMS surfaces in terms of the curing agent-silicone base ratio. There is a peak around 1:10 ratio, which is the stoichiometric ratio recommended by the supplier. Red circle symbols represent the two-layer PDMS surfaces. The error bars are the standard deviation of the acquired measurements.

In Fig. 2, we plot the ACA and RCA values in terms of the curing agent-silicone base ratio. For those surfaces containing high-moderate curing agent concentration (3:1–1:5), the ACA values were all similar. Above 1:5 ratios, the ACA increases as the curing agent ratio decreases. Similarly, the RCA remains nearly constant for surfaces containing more curing agent (3:1–1:5), while for lower curing agent concentrations the RCA decreases for decreasing curing agent concentration. The PDMS 1:1 surface reveals the lowest ACA and highest RCA. This leads to the minimum Contact Angle Hysteresis (CAH) observed. For this reason, water drops will be less retained on this surface [24,25]. It is known that CA is strongly influenced by surface morphology (changes in surface
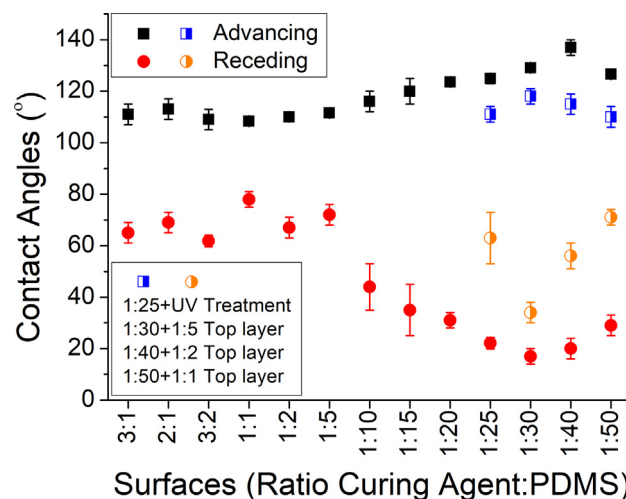

Fig. 2. Advancing and receding contact angles for the PDMS surfaces with different curing agent-to-silicone base ratios. Blue and orange semi-solids symbols represent the two-layer PDMS surfaces. The error bars are the standard deviation of the acquired measurements.

Table 1
Roughness parameters and ice adhesion strength of the rigid surfaces.

Surfaces	R_a (μm)	R_q (μm)	Tensile (kPa)	Shear (kPa)
Hydrophilic	0.35 ± 0.07	0.47 ± 0.11	97 ± 19	480 ± 130
Hydrophobic	0.40 ± 0.09	0.51 ± 0.14	47 ± 20	190 ± 40
Superhydrophobic	5.4 ± 0.5	6.6 ± 0.6	470 ± 60	greater than 800

morphology may lead to Wenzel to Cassie-Baxter transitions) [26]. In our case, the influence of surface morphology is expected to be negligible because all surfaces are very smooth and far from this transition. Drops are resting in the Wenzel state, so morphology does not play a role in the variability of the wetting properties that were found between the surfaces.

The ice adhesion strength in terms of the curing agent-PDMS ratio is plotted in Fig. 3. The adhesion strength in tensile mode is systematically higher than the one measured in shear mode, opposite to our observation for rigid surfaces (see Table 1). This difference may be explained by the different detachment process on elastic surfaces due to their intrinsic deformability. For the tensile ice adhesion strength, we observed the maximum values over the range 1:10–1:30. This observation disagrees with the elastic moduli values, since they decreased at this range. In contrast, the maximum tensile adhesion values correlate reasonably well with the reduction observed in the RCA values from 1:10 to 1:30 (Fig. 2). For very low curing agent concentrations (range 1:40–1:50), there is a clear decrease of tensile adhesion which can be justified by the decrease of the elastic moduli but also by the observed increase of RCA values. It is well-accepted that high RCA typically leads to easy release of water (and ice) from the solid [27]. For high-moderate curing agent concentrations (3:1–1:5), we observe an increase of tensile adhesion upon addition of silicone base. This can be justified by the increase of the elastic moduli observed in the range, while approximately constant RCA, reaching the global minimum for the highest curing agent concentration (the surface 3:1). A local minimum is reached for the ratio 1:1, which can be attributed to the maximum value of RCA observed in this study.

For the ice adhesion strength in shear mode (shear adhesion), the trends were similar, but the maximum adhesion value was observed for the surface 1:10. In addition, the shear adhesion decreases over the range 1:10–1:30, unlike the tensile adhesion. However, the surface hydrophobicity (high RCA or low CAH) and deformability (low E) lead to reduce both, tensile and shear ice adhesion strengths. If we compare the ratios 1:20 and 1:2, which showed very similar E values (1.67 ± 0.10 MPa) but different RCA values ($31 \pm 3°$ and $67 \pm 4°$, respectively), the role of surface wettability is clear. An increase of RCA (less CAH) produces lower adhesion values, approximately the half in this case. Similarly, the comparison between the PDMS 1:5 and PDMS 1:50 + 1:1 surfaces, which have very similar RCA (about $72 \pm 4°$) but different

E values (2.36 ± 0.16 and 0.43 ± 0.04 MPa, respectively), shows that decreasing E clearly reduces ice adhesion.

In summary, the ice adhesion results showed that elastic surfaces have a considerable low ice adhesion strength in shear mode with values below 100 kPa, which is the limit usually considered as low ice adhesion [28,29]. In tensile mode, the surfaces often present "low ice adhesion" strengths (over 120 kPa), which are not far from the values observed for rigid surfaces (see Table 1). However, when both the elastic and hydrophobic properties are improved, these elastic surfaces may reach significantly low ice adhesion values. The PDMS surface 1:50 presents a very low ice adhesion strength in shear mode (17.8 ± 2.4 kPa) due to the low elastic modulus. Instead, the PDMS surface 1:1 has low ice adhesion (22 ± 6 kPa) in both tensile and shear modes, due to its moderate elastic modulus and hydrophobicity. Finally, the PDMS surfaces 1:50 + 1:1 and 3:1 combine both properties, presenting the lowest ice adhesion values in both modes. The PDMS surface 3:1 reveals ice adhesion strengths below 10 kPa, which is assumed to be the limit of super low ice adhesion [28,29].

We postulate that shear adhesion mostly depends on the elastic modulus while tensile adhesion is more influenced by RCA values. To demonstrate this, we conducted the experiments on surfaces that were fabricated by combining different coatings aimed to reach optimal elasticity (bottom coating) with optimal wetting properties (top coating). We fabricated three PDMS surfaces with two layers: 1:30 + 1:5, 1:40 + 1:2 and 1:50 + 1:1. In all cases, the resulting samples showed a small increase of E (Fig. 1), but a noticeable increase of RCA (Fig. 2) with respect to the bottom coating. These two-layers surfaces showed a slight decrease of shear adhesion (see orange markers in Fig. 3), but a noticeable decrease of tensile adhesion (see blue markers in Fig. 3). As expected, the RCA values influences more remarkably the tensile adhesion than the shear adhesion. Similar results are obtained for the PDMS surface treated with UV.

In Fig. 4, we plot the force–time curves measured during a typical pull-off experiment in shear mode. We can observe a clear difference between the detachment mechanisms for rigid and deformable surfaces. The ice detachment is almost instantaneous for rigid surfaces once the peak force is reached. Instead, for elastic surfaces, the release process begins before reaching the peak force and the curve has a round-shape peak. The smoothness of the peak increases as the elastic modulus decreases (see supplementary Videos 1–4).
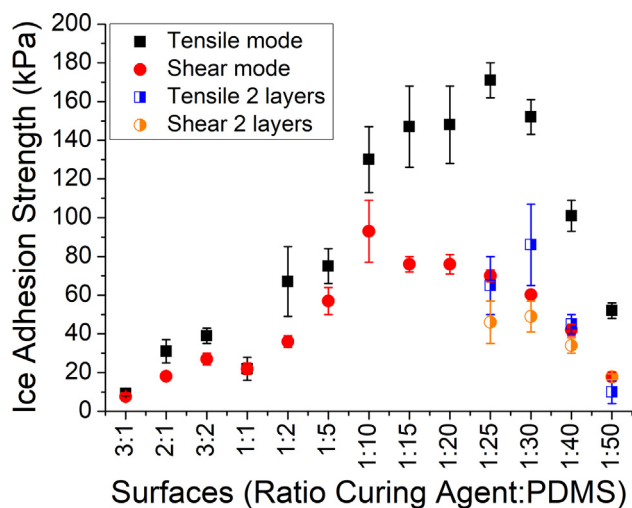

Fig. 3. Ice adhesion strength in the tensile and shear modes for the PDMS surfaces with different curing agent to silicone base ratios. Blue and orange semi-solid symbols represent the two-layer PDMS surfaces.
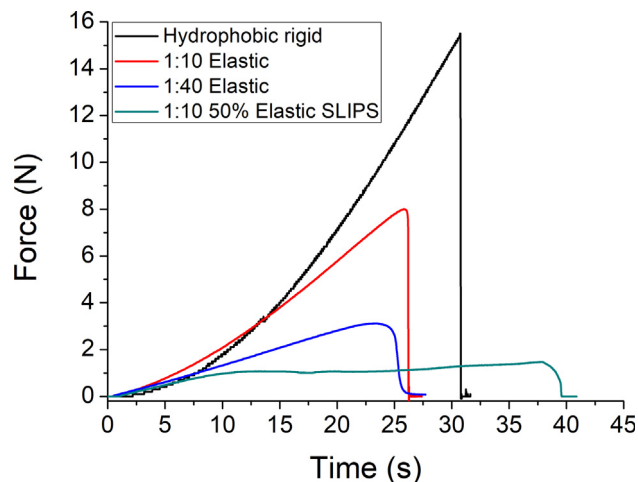

Fig. 4. Comparison of different detachment processes depending on the material elasticity and the presence of interfacial oil. The instrumental error is 0.01 N for the elastic surfaces and 0.1 N for the rigid surface.
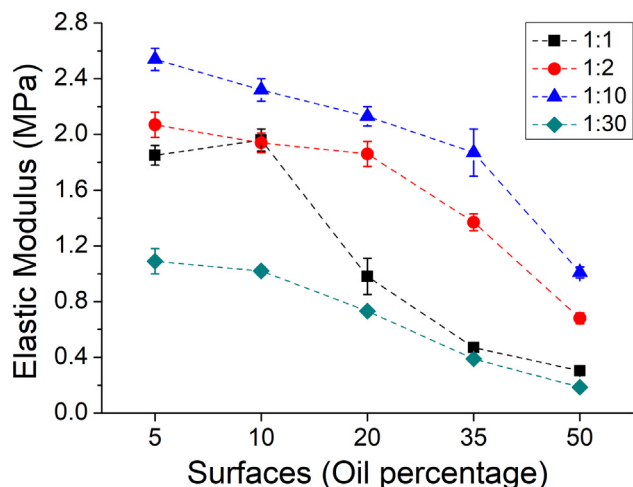
Fig. 5. Elastic moduli of the oil-infused PDMS surfaces in terms of oil concentration. The decrease in elastic moduli as the percentage increases is partially caused by the presence of interfacial oil. Lines are only to guide the eye.

3.3. Oil-infused PDMS surfaces

Alike the PDMS surfaces, the oil-infused PDMS surfaces show low roughness degree, which R_q and R_a values are typically lower than 50 nm (see supplementary Table S2). However, in some cases it reaches about 200 nm.

In Fig. 5, we observe the elastic moduli of the oil-infused surfaces. In this case, we did not add cutting fluid to perform the compression measurement because it produced pollution or might modify the chemical composition of the surfaces. This explain why the E values for the oil-infused PDMS surfaces at low oil concentration (5%) are greater than the same PDMS surfaces that were fabricated without oil-infusion (see their values on Fig. 1). However, we noticed that increasing the oil content reduces the elastic modulus. This reduction is mainly due to the decrease of silicone crosslinking, but it can also be attributed to the presence of silicone oil at the interface. See supplementary Figure S2 for a comparison of elastic modulus (E) that was measured with and without cutting fluid on (non-infused) PDMS surfaces.

In Fig. 6, we plotted the values of SA and ACA/RCA in terms of the oil percentage. In overall, the SA decreases, while the RCA increases for increasing oil concentration. This is due to oil is a
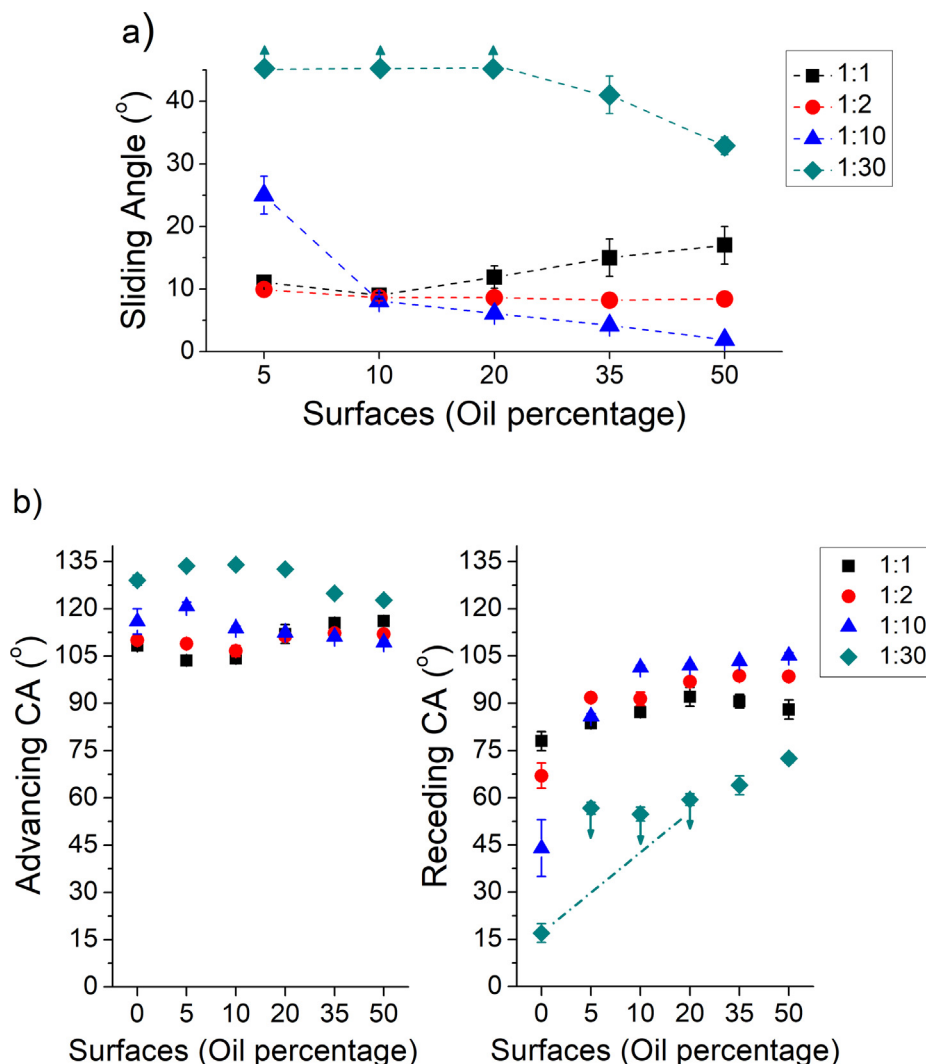

Fig. 6. a) Sliding angle of the oil-infused PDMS surfaces in terms of oil concentration. b) Advancing and receding contact angles of the oil-infused PDMS surfaces. The points with an arrow mean that the value is greater (up arrow) or lower (down arrow) than the limit experimental value. These values are produced with the surface 1:30 at oil percentage lower than 35% because the sessile drops did not slide for tilts above 60°, which is the maximum tilting reached by our apparatus. This way, we only know a maximum value for RCA. The values for none oil-infusion (0%) were obtained with the growing-shrinking drop method.
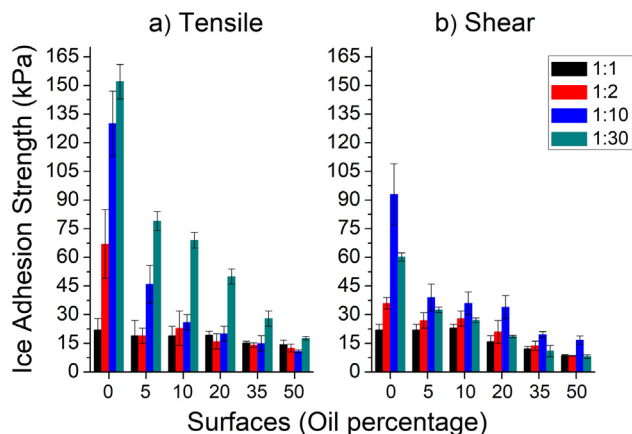
P.F. Ibáñez-Ibáñez, F. Javier Montes Ruiz-Cabello, M.A. Cabrerizo-Vílchez et al.

Journal of Colloid and Interface Science 608 (2022) 792–799

Fig. 7. Ice adhesion strength, in a) tensile and b) shear modes, in terms of oil concentration for the oil-infused PDMS surfaces.

non-polar liquid that increases the hydrophobicity of the material. Moreover, the oil at the interface acts as a lubricant, increasing drops mobility and reducing contact-line pinning. Moreover, we can see that the CAH and the SA are considerably low for many of these surfaces. This low CAH is usually related to high drop mobility [10,27]. High drop mobility based in reduced CAH but with intermediate CAs values is typical of SLIPS [30], which contrast with (super)hydrophobic surfaces that show low CAH but high CAs values [31,32]. From these wettability properties, one might consider the oil-infused surfaces as a type of SLIPS [33].

In Fig. 7, we plot the ice adhesion strength values, in tensile and shear modes, in terms of oil concentration. It is noticeable that the presence of oil makes the adhesion strength decreases significantly, even for low concentrations. This decrease is more remarkable in tensile mode for the surfaces 1:2 5% and 1:10 5%. The main reason for this drop in adhesion values is the enhancement of the hydrophobicity (RCA increase). Increasing oil percentage decreases the ice adhesion values down to 12.5 ± 2.1 kPa and 8.5 ± 0.3 kPa in tensile and shear modes, respectively, for the surface 1:2 50%. This is our surface with the best interplay between elastic modulus and hydrophobicity. The surface 1:1 50% reaches adhesion values comparable to the surface 1:2 50%, but the best candidate is still surface 1:2 50% because it is "harder", so it might incorporate better mechanical durability.

4. Discussion

4.1. Ice release mechanism on elastic PDMS surfaces

As seen in Section 3.2, ice detachment on elastic surfaces is mainly promoted by surface deformability. This was clearly noticeable by naked eye while performing the ice detachment experiments using surfaces with different elastic moduli (see supplementary Videos 1–4).

In literature, it is reported that for the ice release from elastic surfaces, the mismatch in strain during stress may produce interface deformation and stress accumulation near the point of force application, which facilitates ice release [34–36]. In addition, Beemer et al [37] found that on soft gels, shear ice detachment is produced by separation pulses (due to air cavities formed by local detachments that propagate on the interface). Thus, the ice slides intermittently on the surfaces (stick–slip behavior). However, this stick–slip mechanism was not generally observed in our experiments. The exception eventually occurred for the PDMS surface 3:1 (see supplementary Figure S3), that showed one of the lowest shear moduli ($G \approx E/3$) of this study. For Golovin et al [38], detach-

ment from elastic surfaces is mainly ruled by interfacial cavitation, that produces abrupt release without slippage (similar to our results).

Otherwise, it has been proposed that, for rigid surfaces, ice adhesion strength depends on surface energy through the work of adhesion W_a. The practical work of adhesion for sessile drops can be estimated as $W_a = \gamma_{LV}(1 + cos\theta_R) \propto 1 + cos\theta_R$, where γ_{LV} is the liquid–vapor surface tension and θ_R the RCA. This way, ice adhesion strength is correlated to drop work of adhesion and would scale linearly as $1 + cos\theta_R$ for rigid surfaces [27]. However, it would be reasonable to correlate ice adhesion strength with both E and W_a. Indeed, various works have related ice adhesion strength (τ) of elastic surfaces with the Kendall equation [39] for solid adhesion, which can be written as $\tau \propto \sqrt{W_a G/t}$, where G is the shear modulus and t the coating thickness [12,34,37,38,40].

From our results, the relation between ice adhesion and $(W_a E)^{1/2}$ is not clear (see supplementary Figure S4). Our data do not fit well with this model. It points out to a complex interplay between W_a and E that hides the true dependence of ice adhesion on each parameter separately. These parameters can counteract one another in reducing ice adhesion for some surfaces. For this reason, we conducted a statistical correlation study [41] to determine how much the ice adhesion (in both modes) is affected by these parameters (W_a and E) and their combination. We found that the tensile ice adhesion is highly correlated with W_a, but its correlation with E is much lower. The shear ice adhesion, on the other hand, is not much correlated with W_a while its correlation with E is high. (See results and further discussion in supplementary-Section 5 and Table S3).

As discussed in Section 3.2, we hypothesized that the tensile ice adhesion seemed to be more influenced by RCA (W_a) than by E, while the shear ice adhesion was more influenced by E. The conducted correlation study confirms our hypothesis. Overall, it is clear that tensile and shear adhesion are differently influenced by both parameters (contact angles and elastic modulus). A plausible explanation is that, during the detachment process in tensile mode, the applied force is more uniformly distributed in the ice-surface interface (or at least at the perimeter), so deformability is not so important. On the contrary, in shear mode, the applied force produces stress accumulation near the applied force point, which may be supported by surface deformability. That stress accumulation promotes ice detachment.

4.2. Ice release mechanism on oil infused PDMS surfaces

For oil-infused PDMS surfaces, the force–time curves are similar to the elastic PDMS surfaces, i.e. with a round-shaped peak that reveals the influence of the elasticity on ice detachment. However, there is a particular case where the ice detachment process reveals a different mechanism. For the PDMS surface 1:10 50% (see Fig. 4), the force–time curve in shear mode does not show a clear peak. There is an approximately constant force for a long period, until the ice is completely detached. This means that the ice block slides for a while over the surface, moving about 5 mm before the total detachment (see supplementary Video 5). This singular ice detachment under shear force is typical of SLIPS and it is justified by the presence of lubricant at the interface.

We also analyzed the statistical correlation for the oil-infused surfaces (see supplementary Table S4). In general, there is a significant correlation of ice adhesion with both parameters W_a and E. However, it is still appreciable a higher correlation of tensile adhesion with W_a, while shear adhesion is more correlated with E. In addition, the presence of oil may reduce the ice adhesion in a manner that is not predicted by W_a or E: the interfacial slippage.

For the PDMS surfaces 1:10 50%, the decrease in ice adhesion can be attributed to a detachment mechanism similar to the one observed on SLIPS. The presence of oil creates a (liquid) barrier interface which reduces the direct contact between the ice and the substrate. It leads to low ice adhesion strength values [10,13]. This adhesion decrease is also attributed to the extremely low shear modulus of the lubricant, which produces ice release by oil cohesive failure. However, this may lead to a poor durability of the coating [37]. Golovin et al [38] proposed that, when the polymeric chains are mobile (for example when the lubricating oil is in the bulk of the polymer matrix), the detachment is produced by interfacial slippage. In their case, the shape of the force–time profiles was similar to the ones observed in our PDMS surface 1:10 50%. However, Golovin et al proposed that surfaces with interfacial slippage behave differently to the lubricated surfaces (SLIPS) during the ice release process. The surfaces that show interfacial slippage would be homogeneous, although some of them may develop phase separation that produces a lubricating layer at the interface. In the first case, the release mechanism would be linked to interfacial slippage with adhesive failure, while in the second case, it would be similar to the detachment mechanism occurring on SLIPS: cohesive failure. Although the durability of these surfaces is out of the scope of this manuscript and will be analyzed in detail in a separate paper, we found that these surfaces are not damaged after a deicing cycle. In addition, other works using similar surfaces pointed out that their durability is acceptable [12,42]. Our PDMS surface 1:10 50%, where oil is clearly observable after fabrication, presents ice sliding due to the lubricating layer, so it can be considered a SLIPS-like surface. However, the other oil-infused surfaces have a force–time curve similar to elastic surfaces, without evidence of ice sliding. The presence of oil microdroplets, or more mobile polymer chains might help the initial ice slippage or local detachment, which promotes ice release. This would add a certain degree of interfacial slippage as proposed in bibliography for this kind of surfaces [35,36]. This way, our surfaces show reduced ice adhesion strength partly due to oil presence and higher polymer chains mobility even though ice sliding was only observed for the surface 1:10 50% which however showed phase separation, more interfacial oil (lubricating layer) and less homogeneity.

5. Conclusions

In this work we measured the ice adhesion strength (shear and tensile) for a wide range of elastic hydrophobic surfaces. Unlike the rigid surfaces, the PDMS surfaces show lower shear ice adhesion strengths than tensile adhesion. Alike for rigid surfaces, we observed that the ice release properties of elastic surfaces are enhanced with surface hydrophobicity: higher RCA produces lower ice adhesion. In addition, we found that the surface deformability also plays an important role. The surfaces with low elastic moduli showed lower ice adhesion strength. Thus, from a proper balance between elasticity (low E values) and hydrophobicity (high RCA values), we were able to prepare surfaces with ice adhesion strength below 10 kPa. These findings agree with the recent progress in the field [29,37,38,40]. Although both properties are interrelated, we conclude that hydrophobicity has more influence in reducing the tensile ice adhesion, whereas elasticity is more important in reducing the shear ice adhesion.

In addition, we also explored the impact of adding silicone oil to the elastomeric polymer matrix on the ice adhesion strength. We concluded that the ice adhesion may be substantially reduced with the addition of low-surface tension oil. We found that the improvement on the ice release properties of oil-infused surfaces might be explained mainly by three factors: increase of hydrophobicity,

decrease of elastic modulus and the so-called interfacial slippage, which is originated by the higher surface mobility of polymer chains and the presence of oil microdroplets. This mechanism evokes the ice detachment process on SLIPS. We found that the surfaces with an oil percentage ∼ 50% reveal a greater reduction of ice adhesion. We expanded the range of elasticity, wettability or oil content studied in other works [13,35,36]. Moreover, the oil-infused surfaces can be more homogeneous or undergo a certain degree of phase separation depending on the oil content and polymer crosslinking balance. We confirm that it is possible to prepare oil-infused surfaces without oil segregation after aging, even at high oil percentages, as happens with the PDMS 1:2 50% surface. The opposite phenomenon is achieved for the surfaces 1:10 with more than 35% oil. While the surfaces with oil segregation may have self-healing properties, more stable surfaces may present better durability results under certain environments such as intensive rainfall conditions. Further work should be addressed to examine the applicability of elastic surfaces, especially in terms of their durability properties.

CRediT authorship contribution statement

Pablo F. Ibáñez-Ibáñez: Conceptualization, Investigation, Methodology, Formal analysis, Visualization, Writing – original draft. **F. Javier Montes Ruiz-Cabello:** Conceptualization, Writing – review & editing, Supervision. **Miguel A. Cabrerizo-Vílchez:** Resources, Funding acquisition, Project administration. **Miguel A. Rodríguez-Valverde:** Conceptualization, Writing – review & editing, Supervision, Funding acquisition, Project administration.

Declaration of Competing Interest

The authors declare that they have no known competing financial interests or personal relationships that could have appeared to influence the work reported in this paper.

Acknowledgements

Appendix A. Supplementary material

Supplementary data to this article can be found online at https://doi.org/10.1016/j.jcis.2021.10.005.

References

[1] R. Carriveau, A. Edrisy, P. Cadieux, R. Mailloux, Ice adhesion issues in renewable energy infrastructure, J. Adhes. Sci. Technol. 26 (4-5) (2012) 447–461, https://doi.org/10.1163/016942411X574592.

[2] B.P. Jelle, The challenge of removing snow downfall on photovoltaic solar cell roofs in order to maximize solar energy efficiency - Research opportunities for the future, Energy Build. 67 (2013) 334–351, https://doi.org/10.1016/j.enbuild.2013.08.010.

[3] Y. Cao, W. Tan, Z. Wu, Aircraft icing: an ongoing threat to aviation safety, Aerosp. Sci. Technol. 75 (2018) 353–385, https://doi.org/10.1016/j.ast.2017.12.028.

[4] C.C. Ryerson, Ice protection of offshore platforms, Cold Reg. Sci. Technol. 65 (1) (2011) 97–110, https://doi.org/10.1016/j.coldregions.2010.02.006.

[5] Y. Ibrahim, R. Kempers, A. Amirfazli, 3D printed electro-thermal anti- or de-icing system for composite panels, Cold Reg. Sci. Technol. 166 (2019) 102844, https://doi.org/10.1016/j.coldregions.2019.102844.

[6] J. Liu, J. Wang, H. Memon, Y. Fu, T. Barman, K.S. Choi, X. Hou, Hydrophobic/icephobic coatings based on thermal sprayed metallic layers with subsequent surface functionalization, Surf. Coatings Technol. 357 (2019) 267–272, https://doi.org/10.1016/j.surfcoat.2018.10.002.

[7] Y. Zhuo, S. Xiao, A. Amirfazli, J. He, Z. Zhang, Polysiloxane as icephobic materials – The past, present and the future, Chem. Eng. J. 405 (2021) 127088, https://doi.org/10.1016/j.cej.2020.127088.

[8] R. Zhang, P. Hao, X. Zhang, F. He, Supercooled water droplet impact on superhydrophobic surfaces with various roughness and temperature, Int. J. Heat Mass Transf. 122 (2018) 395–402, https://doi.org/10.1016/j.ijheatmasstransfer.2018.01.076.

[9] L. Boinovich, A.M. Emelyanenko, V.V. Korolev, A.S. Pashinin, Effect of wettability on sessile drop freezing: When superhydrophobicity stimulates an extreme freezing delay, Langmuir 30 (6) (2014) 1659–1668, https://doi.org/10.1021/la403796g.

[10] P. Kim, T.-S. Wong, J. Alvarenga, M.J. Kreder, W.E. Adorno-Martinez, J. Aizenberg, Liquid-infused nanostructured surfaces with extreme anti-ice and anti-frost performance, ACS Nano 6 (8) (2012) 6569–6577, https://doi.org/10.1021/nn302310q.

[11] K. Rykaczewski, S. Anand, S.B. Subramanyam, K.K. Varanasi, Mechanism of frost formation on lubricant-impregnated surfaces, Langmuir 29 (17) (2013) 5230–5238, https://doi.org/10.1021/la400801s.

[12] Z. He, Y. Zhuo, J. He, Z. Zhang, Design and preparation of sandwich-like polydimethylsiloxane (PDMS) sponges with super-low ice adhesion, Soft Matter 14 (23) (2018) 4846–4851, https://doi.org/10.1039/C8SM00820E.

[13] L. Zhu, J. Xue, Y. Wang, Q. Chen, J. Ding, Q. Wang, Ice-phobic coatings based on silicon-oil-infused polydimethylsiloxane, ACS Appl. Mater. Interfaces. 5 (10) (2013) 4053–4062, https://doi.org/10.1021/am400704z.

[14] T. Li, P.F. Ibáñez-Ibáñez, V. Håkonsen, J. Wu, K.e. Xu, Y. Zhuo, S. Luo, J. He, Z. Zhang, Self-Deicing Electrolyte Hydrogel Surfaces with Pa-level Ice Adhesion and Durable Antifreezing/Antifrost Performance, ACS Appl. Mater. Interfaces. 12 (31) (2020) 35572–35578, https://doi.org/10.1021/acsami.0c06912.

[15] F.J.M. Ruiz-Cabello, P.F. Ibáñez-Ibáñez, J.F. Gómez-Lopera, J. Martínez-Aroza, M. Cabrerizo-Vílchez, M.A. Rodríguez-Valverde, Testing the performance of superhydrophobic aluminum surfaces, J. Colloid Interface Sci. 508 (2017) 129–136, https://doi.org/10.1016/j.jcis.2017.08.032.

[16] F.J. Montes Ruiz-Cabello, P. Ibañez-Ibañez, G. Paz-Gomez, M. Cabrerizo-Vilchez, M.A. Rodriguez-Valverde, Fabrication of Superhydrophobic Metal Surfaces for Anti-Icing Applications, J. Vis. Exp. (2018), https://doi.org/10.3791/57635 e57635.

[17] Z. Wang, A.A. Volinsky, N.D. Gallant, Crosslinking effect on polydimethylsiloxane elastic modulus measured by custom-built compression instrument, J. Appl. Polym. Sci. 131 (22) (2014) n/a–n/a, https://doi.org/10.1002/app.41050.

[18] I.D. Johnston, D.K. McCluskey, C.K.L. Tan, M.C. Tracey, Mechanical characterization of bulk Sylgard 184 for microfluidics and microengineering, J. Micromechanics Microengineering. 24 (3) (2014) 035017, https://doi.org/10.1088/0960-1317/24/3/035017.

[19] F.J.M. Ruiz-Cabello, M.A. Rodríguez-Valverde, M. Cabrerizo-Vílchez, A new method for evaluating the most stable contact angle using tilting plate experiments, Soft Matter 7 (2011) 10457–10461, https://doi.org/10.1039/C1SM06196H.

[20] C.L. Moraila-Martínez, F.J. Montes Ruiz-Cabello, M.A. Cabrerizo-Vílchez, M.A. Rodríguez-Valverde, The effect of contact line dynamics and drop formation on measured values of receding contact angle at very low capillary numbers, Colloids Surfaces A Physicochem. Eng. Asp. 404 (2012) 63–69, https://doi.org/10.1016/J.COLSURFA.2012.04.012.

[21] E. Pierce, F.J. Carmona, A. Amirfazli, Understanding of sliding and contact angle results in tilted plate experiments, Colloids Surfaces A Physicochem. Eng. Asp. 323 (1-3) (2008) 73–82, https://doi.org/10.1016/j.colsurfa.2007.09.032.

[22] C.W. Extrand, Y. Kumagai, An experimental study of contact angle hysteresis, J. Colloid Interface Sci. 191 (2) (1997) 378–383, https://doi.org/10.1006/jcis.1997.4935.

[23] J. Vaicekauskaite, P. Mazurek, S. Vudayagiri, A.L. Skov, Mapping the mechanical and electrical properties of commercial silicone elastomer formulations for stretchable transducers, J. Mater. Chem. C. 8 (4) (2020) 1273–1279, https://doi.org/10.1039/C9TC05072H.

[24] L. Gao, T.J. McCarthy, Teflon is hydrophilic, Comments on definitions of hydrophobic, shear versus tensile hydrophobicity, and wettability characterization, Langmuir. 24 (17) (2008) 9183–9188, https://doi.org/10.1021/la8014578.

[25] C.G.L. Furmidge, Studies at phase interfaces. I. The sliding of liquid drops on solid surfaces and a theory for spray retention, J. Colloid Sci. 17 (4) (1962) 309–324, https://doi.org/10.1016/0095-8522(62)90011-9.

[26] A.R. Esmaeili, N. Mir, R. Mohammadi, A facile, fast, and low-cost method for fabrication of micro/nano-textured superhydrophobic surfaces, J. Colloid Interface Sci. 573 (2020) 317–327, https://doi.org/10.1016/J.JCIS.2020.04.027.

[27] A.J. Meuler, J.D. Smith, K.K. Varanasi, J.M. Mabry, G.H. McKinley, R.E. Cohen, Relationships between water wettability and ice adhesion, ACS Appl. Mater. Interfaces. 2 (11) (2010) 3100–3110, https://doi.org/10.1021/am1006035.

[28] M.J. Kreder, J. Alvarenga, P. Kim, J. Aizenberg, Design of anti-icing surfaces: smooth, textured or slippery?, Nat Rev. Mater. 1 (2016) 1–15, https://doi.org/10.1038/natrevmats.2015.3.

[29] Z. He, S. Xiao, H. Gao, J. He, Z. Zhang, Multiscale crack initiator promoted super-low ice adhesion surfaces, Soft Matter 13 (37) (2017) 6562–6568, https://doi.org/10.1039/C7SM01511A.

[30] T.-S. Wong, S.H. Kang, S.K.Y. Tang, E.J. Smythe, B.D. Hatton, A. Grinthal, J. Aizenberg, Bioinspired self-repairing slippery surfaces with pressure-stable omniphobicity, Nature 477 (7365) (2011) 443–447, https://doi.org/10.1038/nature10447.

[31] M. Sun, C. Luo, L. Xu, H. Ji, Q.i. Ouyang, D. Yu, Y. Chen, Artificial lotus leaf by nanocasting, Langmuir 21 (19) (2005) 8978–8981, https://doi.org/10.1021/la050316q.

[32] M. Miwa, A. Nakajima, A. Fujishima, K. Hashimoto, T. Watanabe, Effects of the surface roughness on sliding angles of water droplets on superhydrophobic surfaces, Langmuir 16 (13) (2000) 5754–5760, https://doi.org/10.1021/la991660o.

[33] J. Cui, D. Daniel, A. Grinthal, K. Lin, J. Aizenberg, Dynamic polymer systems with self-regulated secretion for the control of surface properties and material healing, Nat. Mater. 14 (2015) 790–795, https://doi.org/10.1038/nmat4325.

[34] C. Wang, T. Fuller, W. Zhang, K.J. Wynne, Thickness dependence of ice removal stress for a polydimethylsiloxane nanocomposite: sylgard 184, Langmuir 30 (43) (2014) 12819–12826, https://doi.org/10.1021/la5030444.

[35] Y.H. Yeong, A. Milionis, E. Loth, J. Sokhey, Self-lubricating icephobic elastomer coating (SLIC) for ultralow ice adhesion with enhanced durability, Cold Reg. Sci. Technol. 148 (2018) 29–37, https://doi.org/10.1016/j.coldregions.2018.01.005.

[36] Y.H. Yeong, C. Wang, K.J. Wynne, M.C. Gupta, Oil-infused superhydrophobic silicone material for low ice adhesion with long-term infusion stability, ACS Appl. Mater. Interfaces. 8 (46) (2016) 32050–32059, https://doi.org/10.1021/acsami.6b11184.

[37] D.L. Beemer, W. Wang, A.K. Kota, Durable gels with ultra-low adhesion to ice, J. Mater. Chem. A. 4 (47) (2016) 18253–18258, https://doi.org/10.1039/C6TA07262C.

[38] K. Golovin, S.P.R. Kobaku, D.H. Lee, E.T. DiLoreto, J.M. Mabry, A. Tuteja, Designing durable icephobic surfaces, Sci. Adv. 2 (3) (2016) e1501496, https://doi.org/10.1126/sciadv.1501496.

[39] K. Kendall, The adhesion and surface energy of elastic solids, J. Phys. D. Appl. Phys. 4 (1971) 1186–1195, https://doi.org/10.1088/0022-3727/4/8/320.

[40] P. Irajizad, S. Nazifi, H. Ghasemi, Icephobic surfaces: definition and figures of merit, Adv. Colloid Interface Sci. 269 (2019) 203–218, https://doi.org/10.1016/j.cis.2019.04.005.

[41] D.Y. Kwok, T. Gietzelt, K. Grundke, H.-J. Jacobasch, A.W. Neumann, Contact Angle Measurements and Contact Angle Interpretation. 1. Contact Angle Measurements by Axisymmetric Drop Shape Analysis and a Goniometer Sessile Drop Technique, Langmuir 13 (10) (1997) 2880–2894, https://doi.org/10.1021/la9608021.

[42] Y. Zhuo, F. Wang, S. Xiao, J. He, Z. Zhang, One-Step Fabrication of Bioinspired Lubricant-Regenerable Icephobic Slippery Liquid-Infused Porous Surfaces, ACS Omega 3 (8) (2018) 10139–10144, https://doi.org/10.1021/acsomega.8b01148.